DOI: https://doi.org/10.54966/jreen.v27i2.1190

Journal of Renewable Energies

Revue des Energies Renouvelables

journal home page: https://revue.cder.dz/index.php/rer

Research paper

Charge carrier mobility and the recombination processes within a bulk heterojunction organic solar cell exhibiting disordered hopping

Teneng Assah Mbanga [a], **David Afungchui** [b,*] **Joseph Ebobenow** [c], **Ali Helali** [d] **and Nkongho Ayuketang Arreyndip** [e]

[a,b] *Department of Physics, Faculty of Sciences, The University of Bamenda, Bambili, NWR, Cameroon.*

[c] *Department of Physics, Faculty of Sciences, University of Buea, SWR, Cameroon.*

[d] *National Engineering School of Sousse, Higher Institute of Transport and Logistics, Mechanical Laboratory, University of Sousse, Riadh City, Sousse, Tunisia.*

[e] *Potsdam Institute for Climate Impact Research (PIK), Potsdam, Germany.*

ARTICLE INFO

Article history:

Received May 3rd, 2024

Accepted December 18, 2024

Keywords:

Drift-diffusion,
Charge carrier mobility,
Recombination processes,
Bulk heterojunction,
Organic solar cell,
Disordered hopping.

ABSTRACT

This paper studies the interplay between charge carrier mobility and the related recombination processes exhibited within a bulk heterojunction-disordered hopping organic solar cell, using drift-diffusion simulations. The investigation focuses on the recombination order, the current-voltage properties and the charge carrier mobility's active involvement in the recombination processes within an organic solar cell. The outcome of the investigation based on the drift diffusion simulation highlights the fact that the recombination characteristics are altered by charge carrier mobility. There exists a normalised mobility, which averages the progression of slow to fast charge carriers transforming the electrons and holes mobilities into an optimal mobility, which significantly increases the efficiency for a variety of bulk heterojunction structure types by significantly lowering the extent of recombination.

1. INTRODUCTION

An organic solar cell is an application of photovoltaic (PV) technology based on the use of organic materials which are more easily available and cheaper compared to their inorganic counterparts. Unlike fossil fuels which are fast depleting and at the same time detrimental both to the environment and adversely affecting the world's climate, organic solar cells provide an inexhaustible and clean energy.

* *Corresponding author, E-mail address: afungchui@yahoo.fr*
Tel : + 237654785555

ISSN: 1112-2242 / EISSN: 2716-8247

Photovoltaic (PV) technology is fast expanding and establishing itself as the most dominant carbon-free source of electricity generation. Inorganic semiconductor materials made mostly of a combination of group three and five elements of the periodic table find widespread applications in conducting areas of commercial photovoltaic applications (Mahmud et al., 2018). Even though the efficiency of inorganic PV has experienced a drastic increase in recent years, the technology remains expensive partly because of the raw materials used and their purification processes often requiring very high temperatures (Galagan & Andriesse, 2012).

As a remedy to the high cost, organic photovoltaic (OPV) solar cell technology uses engineered organic compounds equipped with the ability to capture photons and stimulate the movement of charges leading to the flow of current that can be harnessed. The use of organic photovoltaic (OPV) materials is more advantageous in that low temperatures are used in the fabrication processes, the materials exhibit low density, and they are flexible to bending and permit roll-to-roll printing. All of these properties result in both low-cost and low-weight devices. It is believed that organic photovoltaic (OPV) cells will supersede their inorganic counterparts in the foreseeable future once the efficiency is upgraded to a comparable level. OPV is a renewable energy technology, consequently, it is non-polluting, environmentally friendly, has a low cost in fabrication, operation and maintenance, operates at ambient temperatures, incurs low operational cost, enjoys high public acceptance and has a high safety record (Chen, 2019; Sharma et al., 2022). The low weight of OPV cells in their varieties from hybrid perovskites to totally organic polymers gives them the edge to be more suitable for space applications and to fully replace their inorganic counterparts. These OPV materials are particularly suitable because their properties can be sharply improved through a diversity of chemical syntheses.

Historically, the stage for OPV research was set by Alfredo Pochettino as early as 1906, who studied the photoconductivity of anthracene (Dastoor & Belcher, 2019). This spurred the interest of the scientific community to intensify the study of photoconductivity in organic molecules and some organic semiconductors started emerging in the 1970s. The first single-layer OPV cell with an efficiency of 1% was produced by Tang (1986). It consisted of two materials forming a junction; copper phthalocyanine which was an electron-accepting material and a perylenetetracarboxylic derivative which was a hole-transporting material (Forrest, 2012; Y. Li et al., 2022). From this starting point other architectures have emerged which consist of the: bulk heterojunction organic solar cells, perovskite solar cells, multijunction organic solar cells, and the bilayer organic solar cells.

The selection of the appropriate materials for building an organic solar cell, especially the bulk heterojunction type is crucial both in regulating the recombination process and in improving its efficiency (Duan & Uddin, 2020). Some materials that have been used so far include fullerene derivatives like ICBA, PC61BM, bisPC61BM, and PC71BM. These present an advantage as good electron acceptors but fall short in their low efficiency (Li et al., 2022). In 2015, non-Fullerene acceptors were discovered to present improved characteristics as compared to their Fullerene counterparts. These include molecules like ITIC, (Zhao et al., 2016, 2017; Xu et al., 2018; S. Li et al., 2016; Wang et al., 2018; Lin et al., 2015, 2016) Y6, (Yuan, Zhang, et al., 2019; Tran et al., 2020) and L8-BO (Song et al., 2021; C. Li et al., 2021); in addition to perylene diimide(PDI) (Guo et al., 2016, 2017; Zhan et al., 2007), naphthalene diimide (NDI) (Fan et al., 2017; Gao et al., 2016; Mori et al., 2014), bithiophene imide (BTI) (Shi et al., 2020; Sun et al., 2020), and B←N-bridged bipyridine (BN- Py) (Zhao et al., 2020) which are habitual building blocks for non-fullerene acceptors of polymer photovoltaic cells. These have significantly enhanced charge carriers' mobility and recombination properties. Efficient enhancing donor materials are also being used; these include: PDBT-T, (Xu et al., 2018; Yuan, Huang, et al., 2019; Zhao et al., 2016, 2017), PM6, (Zhang et al., 2018 ; Cui et al., 2020; Zhang, et al., 2019; Yuan,) PM7, (Zhang et al., 2018 ; Ma et al., 2020), D18 (Liu et al., 2020 ; Jin et al., 2021). Ternary blends of OPV cells which are composed of either one donor and two acceptors or one acceptor and two donors are

followed by the quaternary blends (Xu et al., 2017; Qin et al., 2021; Goh et al., 2016; Bi et al., 2019;). With this range of materials, the OPV cells have witnessed a drastic improvement in their efficiency (Hong et al., 2020). Nonetheless, the occurrence of recombination experienced in these molecules persists since non-fullerene derivative acceptor molecules are highly susceptible to exhibiting low mobility of charge carriers in the interval $10^{-9} - 10^{-8} m^2 V^{-1} s^{-1}$ (Göhler et al., 2018).

Nonetheless, experience has shown that the efficiency of an organic solar cell is inversely proportional to the rate of charge recombination. So a very low charge recombination rate is required to improve the efficiency. An earlier study (Wilken et al., 2021) has highlighted the fact that the rate of charge recombination in OPV cells is mostly dependent on three factors, which are: phase purity, crystalline quality and molecular order and independent of the structure and the extent of the phase separation. This however warrants an in-depth investigation because the rate of recombination through the bulk also depends on charge mobility. It is also worth noting that recombination can happen in trap states located in the band gap interface (Bi et al., 2019; Dastoor & Belcher, 2019; Hong et al., 2020). Three factors have been identified to generate localized trap states in the band gap with non-identical properties. These include: Heighten illumination, thermal annealing and fullerene doping. These states can be localized either midway in the band gap interface or they can be band tail states or still they can be shallow states (Street et al., 2012). It has also been observed that the selection of electrode used will influence the number of interfacial recombinations if comparable rates of bulk recombination are retained and for the best option of electrodes, ZnO was identified (Schopp et al., 2022). Considering the case of mobility as it relates to the bimolecular carrier recombination coefficient, k, the effective mobility was correlated to the experimentally measured charge carrier mobilities and the results were compared with those of recombination models that depend on the morphology of the bulk heterojunction. The study established that the mobilities of the charge carriers taken into consideration separately correlates with k in an arithmetic, geometric or harmonic progression based on the size of the localized domains inside a bulk heterojunction (Vollbrecht et al., 2020). This provided support to an investigation that was carried out by (Vollbrecht et al., 2023) on a variety of solar cells to correlate effective mobility to the photo-conductance mobilities under open circuit conditions using a broad range of carrier densities, to guarantee that the hole and electron mobilities were balanced.

Therefore, the goal of this paper is to fine-tune the analysis of recombination in an organic solar cell by examining the recombination order through the drift and diffusion perspectives, and current-voltage characteristic factors in the context of synchronizing electron and hole charge mobility into consistent system mobility. All these are to create affordable, effective, long-lasting and highly efficient organic solar cells.

2. THEORY

2.1 Charge carrier generation and recombination processes in the heterojunction

When two dissimilar organic materials are put together, an effective field is generated leading to the creation of a heterojunction organic solar cell. An organic solar cell generates electricity by creating excitons which are subsequently split into free electron-hole pairs by the effective fields. The lifetime of excitons is very short, measuring nanoseconds and so they dissociate within the interval that the electron makes a transition from the conduction band of the absorber to that of the acceptor molecules.

The active area of the heterojunction is formed by laminating donor and an acceptor materials, ensuring a good contact. When it is illuminated with photons, excitons are generated that can diffuse and eventually dissociate. The overall efficiency and performance of the active area is determined by the

elements that make up the donor/acceptor molecules coupled with the morphology and its eventual stability. (Wagenpfahl et al., 2010; Volpi, 2017).

Exciton Lifetime: This is the time lapse from the creation of an exciton until its eventual split and dissociation. An extremely short exciton lifetime will affect the computation of the exciton diffusion process. Depending on the thickness of the heterojunction, the lifetime of the exciton is calculated such that upon dissociation, it will be in the vicinity of the anode where it is picked up while the electron gets to the cathode. A larger heterojunction will require more photon energy. It is recommended for organic semiconductors to be moderately large or thick because of the relatively short exciton lifetime.

The following structures of organic solar cells can be identified: the single layer, the bilayer or the bulk heterojunction. Energetically the single-layer organic solar cell is separated by the HOMO-LUMO band structure. It is made up of an anode and a cathode, each of which has its work function, with the cathode connected to the HOMO-LUMO band. The anode is transparent for easy transmission of light to the semiconductor where it is absorbed creating an exciton which eventually splits into an electron-hole pair approximately of the order of the HOMO-LUMO bond energy. Excitons may not readily split but rather diffuse in the event where the binding energy is big. The thickness of the semiconductor is estimated from the knowledge of the exciton diffusion length. We note that the efficiency of a single-layer organic solar cell is very low (Shaabani et al., 2012).

Bilayer organic solar cells are made of two organic materials having a discontinuity layer in between them which ensures that excitons dissociate before reaching the cathode. One of the materials equipped with a hole-transporting layer is connected to the anode while the other equipped with an electron-transporting layer is connected to the cathode. Light incident on the anode creates an exciton that diffuses to the discontinuous layer where it splits up and the resulting electron and hole are separately picked up at the cathode and anode respectively. Bilayer OPV enjoys a higher efficiency because the structure of both layers is engineered to ensure that the heterojunction coincides with the exciton diffusion length in both layers (Shaabani et al., 2012).

A bulk heterojunction (BHJ) organic solar cell is made up of an interblend of an electron-transporting semiconductor and a hole-transporting semiconductor. The two semiconductor types, at the same time, have many interphases between them. The dissociation of excitons is facilitated once they are generated because they can diffuse in any direction with high chances of meeting one of these numerous interphases. Once the exciton splits in an interphase, the electron is collected by the two electrodes. Blending assists in a larger heterojunction surface resulting in a higher efficiency (Mandal et al., 2012).

The efficiency of organic solar cells remains low compared to that of their inorganic counterpart because of the number of losses encountered at every stage of the process. Light absorption by the photoactive material is not very efficient due to finite thickness. Also, the process of generation of free-charge carriers incurs some losses. The resulting recombination process can be one of the following: Excitons Recombination; geminate recombination; non-geminate recombination and the discrepancy between solar spectrum and material absorptivity.

Excitons recombination occurs when the excitons created in the photoactive layer, in the course of their diffusion recombine before reaching the donor/acceptor interface. In the case of geminate recombination, the exciton upon dissociation at the donor/acceptor interface constitutes an electron-hole pair that is clasped by the generated Coulombic force of attraction. The internal built-in field superposed to the applied voltage, causes the efficiency to be lowered because the photocurrent is going to depend strongly on the voltage (Abudulimu, 2012). Non-germinate recombination occurs after exciton dissociation where the free charge carriers move to specific electrodes and recombine as a result of an

electrical field (Zheng et al., 2017). In trap-assisted recombination, trap states confine the charge carriers which can either recombine or be liberated based on the energy levels of the traps.

2.2 Langevin and Shockley-Read-Hall (SRH) Recombination concept

Here the processes involved are the bimolecular and trap-assisted recombinations. According to Langevin-type theory, the diffusion of charges with opposing signs in their Coulombic attraction is the slowest step. β_L, the coefficient that describes the Langevin recombination process is expressed as:

$$\beta_L = \frac{e}{\varepsilon_0 \varepsilon}(\mu_+ + \mu_-) \tag{2.1}$$

Where e is the electronic charge and $\mu_+(\mu_-)$is the hole (electron) mobility.

The SRH process proceeds in two steps such that trapped charges recombine with those of the opposite sign. Two steps are involved in the SRH process, of which the slower step that determines the overall rate is that of the diffusion of the free carrier to the vicinity of the trapped carriers driven by the Coulombic attraction (Groves et al., 2010; Markus & Anne, 2009). The overall efficiency of an organic solar cell captures contributions from all associated loss mechanisms. These include processes like absorption of photons, transfer of charges and diffusion of excitons, electron-hole pair splitting, transport of charges, and charge collection at the electrodes.

3. MATERIAL AND METHODS

3.1 Drift diffusion model for an organic solar cell

The drift-diffusion equations are developed and simulated to incorporate both computational and physical methods and are intended to capture the events in the mobility and recombination-prone regions in organic solar cells. The model can be used as a tool to investigate multilayer devices having intricate structures that can be harmoniously combined in the framework of diffusion and drift currents. The essence is to have mutually non-interacting and quasi-free charged particles which can be either electrons or holes, that can be described by the continuity equation as presented below.

3.1.1 The drift current

The drift current is derived by applying Newton's laws of motion, where the forces acting on a charged particle are: the electric force given by $E = -eF$ and a frictional force caused by scattering expressed as $F_f = m\,v/\tau$. Where: the quantities v, τ, F, e, and E denote respectively the drift velocity, the average scattering time, electric field strength, the electronic charge, and the electric force. Taking the electric force as the driving force in Newton's law gives the following equation under steady-state conditions:

$$v = -\frac{e\tau}{m}F = -\mu F \tag{3.1}$$

Where μ is the synchronised mobility of both electrons and holes through the minimum and maximum range.

Then the electric current density, j, is next expressed according to the microscopic Ohm's law as:

$$j_{drift} = (-env_n + epv_p) = e(n\mu_n F + p\mu_p F) = \sigma F \tag{3.2}$$

Where: σ is the conductivity, n and p, are the electron and hole densities respectively and the subscripted terms v_n and v_p depict respectively electron and hole average velocity.

3.1.2 The diffusion current

Generated diffusion electric currents are governed by Fick's law expressed as:

$$j_{diff}^{n} = -(-e)D\nabla n \quad and \quad j_{diff}^{p} = -(+e)D\nabla p \tag{3.3}$$

Fick's law states that if diffusion effects are important, then chemical equilibrium is established when concentration gradients drop to zero. Putting this equation in a form similar to "Eq. (3.2)" gives:

$$\nabla n = n\frac{\nabla \xi}{k_B T} \tag{3.4a}$$

Considering the Einstein relation, $D/\mu = k_B T/e$, the diffusion coefficient, D, can be expressed in terms of the mobility leading to the following equation for the total diffusion current:

$$j_{diff} = n\mu_n \nabla \xi_n - p\mu_p \nabla \xi_p \tag{3.4b}$$

3.1.3 Total current

Adding "Eq. (3.4b)" with "Eq. (3.2)" and considering that *F* = -∇∅, where ∅ is the electrical potential, gives:

$$j_n = -n\mu_n e\nabla \emptyset + n\mu_n \nabla \xi_n = n\mu_n \nabla E_F^n \tag{3.5}$$

Where, E_F^n, is the electrochemical potential gradient.

3.2 The Drift -Diffusion Equations

Here the continuity and the drift-diffusion equations are combined to derive the Boltzmann equation. Let $f(r, v, t)$, be a distribution function that describes the state of a particle in a classical ensemble expressed as (Zojer, 2021):

$$(\partial N)_x = (\partial f(x, v_x) d\sigma dx)_x = -\frac{f(x + dx,\ v_x) - f(x,\ v_x)}{dx} dx v_x dt d\sigma \tag{3.6}$$

The right-hand side of the equation simplifies to df/dt and for particles movement in the x direction the resulting rate equation for f is expressed as:

$$\frac{\partial f}{\partial t}|_x = -\frac{\partial f}{\partial x} v_x \tag{3.7}$$

In terms of velocity and acceleration, "Eq. (3.7)" can be rewritten as:

$$\frac{\partial f}{\partial t}|_{v_x} = -\frac{\partial f}{\partial v_x} a_x \tag{3.8}$$

The general change of the distribution function, f, incorporating all the three space coordinates and time, is expressed as:

$$\frac{\partial f}{\partial t} + \mathrm{v}\nabla_r f + \mathrm{a}\nabla_v f \; = \; 0 \tag{3.9}$$

The existence of collisions which cause recombinations, introduces an additional term, $\frac{\partial f}{\partial t}|_{coll}$, and the complete drift-diffusion equation obtained from the momentum method is expressed as:

$$\int v^{\alpha}\left(\frac{\partial f}{\partial t} + v\nabla_r f + a\nabla_v f\right)dv = \int v^{\alpha}\frac{\partial f}{\partial t}|_{coll}dv \tag{3.10}$$

Where "Eq. (3.9)" is multiplied by some power α of v and integrated over v.

The drift and the diffusion equations are obtained by letting $\alpha = 0$. To determine the change in particle density, n(**r**) with time, an integration over all velocities is performed on the distribution function f to get the first term expressed as:

$$\int \frac{\partial f(r,v,t)}{\partial t}dv = \frac{\partial}{\partial t}n(r) \tag{3.11}$$

In the second equation, v and r are independent:

$$\int \nabla_r f(r,v,t)dv \; = \int \nabla_r (f(r,v,t)v)dv = \nabla_r \int vf(r,v,t)dv \tag{3.12}$$

Introducing the mean value of $v(r)$, expressed as $\langle v(r)\rangle = \int vfdv/\int fdv \; = \int vfdv/n(r)$, into "Eq. (3.12)" transforms it to:

$$\nabla_r \int vf(r,v,t)dv = \; \nabla_r(n(r)\langle v(r)\rangle) \; = \; \nabla_r \mathrm{j(r)} \tag{3.13}$$

Where j(r) is the particle current density. In the presence of an applied field F, the third term is proportional to

$$\int_{-\infty}^{\infty} F\nabla_v f dv \tag{3.14}$$

If f is evaluated at infinity and over all possible scattering events (scattering-in and scattering-out) for each velocity, we have zero. Thus, only the first two terms of "Eq. (3.10)" are left and the equation simplifies to:

$$\frac{\partial}{\partial t}n(r) + \nabla_r \mathrm{j(r)} \; = 0 \tag{3.15}$$

Which is referred to as the continuity equation. If α = 1, "Eq. (3.10)" leads to the drift-diffusion equation:

$$n\mu F - \mathrm{D}\nabla_r \mathrm{n} \; = \mathrm{J} \tag{3.16}$$

μ denotes the mobility of charge carriers expressed by $\mu = e\tau_s / m$, where τ_s, D and m denote respectively the scattering time, the diffusivity constant and the mass of the particle. Electrons and holes consist of charge carrier densities denoted respectively as n and p and are distributed on molecules over a large spatial extent. For a typical BHJ organic solar cell, some constraints are placed on its characteristics such as: letting the dimensions of the device to be far greater than the hopping distance while the lifetime of charge carriers is to be such that they can perform multiple hops before recombining. Consequently, the process of charge transport will proceed by the charge carriers hopping in multiple-step. The charge transport current is described by the laws of drift and diffusion and this does not depend on the location of the charge carriers. It is important to note that the parameters (μ and D) in "Eq. (3.16)" are treated as effective parameters because the drift-diffusion method when applied to organic semiconductors, is considered a macroscopic model. (Mandal et al., 2012).

3.3 Einstein Relation

Einstein's relation expresses the charge carrier mobility μ in terms of the diffusion coefficient D or vice versa. In a state of equilibrium, the drift and diffusion forces for a semiconductor layer do cancel each other. However, if an electric field is applied the charges are redistributed. In a similar manner, an initial diffusion current always exists as a result of the diffusion gradient but will stop immediately when a compensating field is set up. When equilibrium is reached, the following equation is applicable for each coordinate direction (which here is x) according to "Eq. 3.16" (Yumnam et al., 2017):

$$n\mu F = \mathrm{D}\frac{\partial n}{\partial x} \tag{3.17}$$

The generalized Einstein relation is obtained by introducing the electrochemical potential η, expressed as:

$$\frac{D}{\mu} = \frac{nF}{\frac{\partial n}{\partial x}} = \frac{nF}{\frac{\partial n}{\partial \eta}\frac{\partial \eta}{\partial x}} = \frac{n}{e\frac{\partial n}{\partial \eta}} \tag{3.18}$$

The quantity η is partly expressed in terms of the x-component of the electric field written as a function of the Potential ($\emptyset = eFx$). In effect, the motion of an electron through a distance dx will cause a proportional change in the electro-chemical potential of magnitude $eFdx$. Because, $\mathrm{n} \propto e^{\frac{\eta}{K_B T}}$, Boltzmann statistics can be applied to, "Eq. (3.18)" above, which then simplifies to:

$$\frac{D}{\mu} = \frac{k_B T}{e} \tag{3.19}$$

This is the classical Einstein relation, which is very useful in the drift-diffusion simulations of semiconductor devices.

3.4 Poisson's equation

Space charge effects are common in low-mobility semiconductors in which free charge carriers can build up to build a space charge. The presence of this space charge will create an electric field F expressed as.

$$\nabla F = \frac{\rho}{\varepsilon_o \varepsilon_r} \tag{3.20}$$

This field equally modifies the electrical potential of the surrounding space, as expressed by Poisson's equation of electrostatics:

$$\Delta\emptyset = -\frac{\rho}{\varepsilon_o \varepsilon_r}(p-n) \tag{3.21}$$

3.5 Differential equation system

The continuity equation is written for both electrons (n) and holes (p) while adding contributions from generation (G) and recombination (R) processes. The resulting coupled differential equations governing organic solar cells according to the drift-diffusion simulations including the effects of space-charges are expressed as:

$$\frac{\partial n}{\partial t} = \mathrm{G} - \mathrm{R} - \frac{1}{-e}\frac{\partial J_n}{\partial x} \tag{3.22}$$

$$\frac{\partial p}{\partial t} = \mathrm{G} - \mathrm{R} - \frac{1}{-e}\frac{\partial J_p}{\partial x} \tag{3.23}$$

Where J_n "Eq. (3.24)" and J_p "Eq. (3.25)" are the current densities.

$$J_n = \mathrm{en}\mu_n \mathrm{F} - (-\mathrm{e})\mathrm{D}\frac{\partial n}{\partial x} \tag{3.24}$$

$$J_p = \mathrm{en}\mu_p \mathrm{F} - \mathrm{eD}\frac{\partial p}{\partial x} \tag{3.25}$$

Poisson's equation "Eq. (3.21)" is next written as below,

$$\frac{\partial^2 \emptyset}{\partial x^2} = -\frac{e}{\varepsilon_0 \varepsilon_r}(\mathrm{p} - \mathrm{n} + N_D^+ - N_A^- + \cdots) \tag{3.26}$$

Where different contributions make up the space charge such as free charge carriers, trapped charge carriers and localized ionized dopants (N_D^+ and N_A^-).

The excitons, s, continuity equation is expressed as in "Eq. (3.27)" below. Exciton density will vary through a combination of causes such as excitons in the excited states relaxing with a lifetime τ and excitons separating or quenching (G_{opt}). The system is also characterised by a gradient in the diffusion current changes, s, in such a way that an exciton diffusion length $L_D = \sqrt{D_\tau}$ is introduced.

$$\frac{\partial s}{\partial t} = G_{opt} - \frac{s}{T} - R_{Sep,Quench} + \frac{L_D^2}{\tau}\frac{\partial^2 s}{\partial x^2} \tag{3.27}$$

The time dependence of the electric field is written as;

$$\frac{\partial F(x)}{\partial t} = -\frac{1}{L}\frac{\partial \emptyset(L)}{\partial t} - \frac{4\pi e}{\varepsilon}\left(J(x) - \frac{1}{L}\int_0^L J(x)dx\right) \tag{3.28}$$

Where L is the length of the device and ∅ is the electric potential.

3.6 Calculation of the electric field

The discretised equation of the electric field F_{if}^{i} between two points i and i + 1, is given by:

$$F_{if}^{i} = \frac{\Delta m}{2\epsilon_o}\left(\sum_{j=1}^{i}\frac{\rho^i}{\varepsilon_r^i} - \sum_{j=i+1}^{N}\frac{\rho^i}{\varepsilon_r^i}\right) + \frac{\rho^{anode}}{\varepsilon_o\varepsilon_r^i} \tag{3.29}$$

where, ε_r is the dielectric constant and ρ^i is the local space charge, consisting of the sum of all charged species at position i

$$\rho^i = p^i - n^i + N_D^{+i} - N_A^{-i} + p_t^i - n_t^i + \cdots \tag{3.30}$$

The electric field F^i at point i is computed through a linear interpolation expressed as:

$$F^i = \frac{F_{if}^{i-1} + F_{if}^{i}}{2} \tag{3.31}$$

The potential difference between the two electrodes (anode and cathode) is obtained by summing over a particular discretized space subjected to the electric field. Two contributions make up this difference in potential: the applied bias voltage V and the built-in voltage V_{bi}. The former emanates from metals with dissimilar work functions. Consequently, the equation below has to be satisfied:

$$\sum_{i=1}^{N} F^i \Delta m = V - V_{bi} \tag{3.32}$$

3.7 Calculation of rates of change

In what follows, the rate of change is approximated as $\frac{\partial}{\partial t} \approx \frac{\Delta}{\Delta t}$. In moving from a position with superscript i to a position with superscript i + 1, the hole density of the transition rate, $\frac{\Delta\, p^{i\to i+1}}{\Delta t}$, is expressed as:

$$\frac{\Delta p^{i\to i+1}}{\Delta t} \approx \frac{\partial p^{i\to i+1}}{\partial t} = \frac{v^i}{\Delta m} p^i \tag{3.33}$$

Where p^i and v^i are respectively the density of charge carriers the corresponding drift velocity at the position with index i and the distance covered by the charge carrier is Δm.

Replacing v^i by the expression of the drift velocity results in:

$$\frac{\partial p_{drift}^{i\to i+1}}{\partial t} = \begin{cases} \frac{\mu_p^i F^i}{\Delta m} p^i & if \quad F^i > 0 \\ 0 & if \quad F^i \le 0 \end{cases} \tag{3.34}$$

This expression indicates the generation of a drift current of holes in the same direction as the electric field. The diffusion velocity is given by

$$v_{diff} = \frac{D_p}{\Delta m} = \frac{\mu_p k_B T}{e\Delta m} \tag{3.35}$$

The introduction of classical Einstein relation "Eq. (3.17)" will result in an equation for the rate of transition of holes caused by diffusion:

$$\frac{\partial p_{diff}^{i\to i+1}}{\partial t} = \frac{\mu_p k_B T}{ed\Delta m^2} p_i \tag{3.36}$$

The field-dependent term brought on by field-assisted hopping also contributes to the drift current in the electric field's direction. This contribution is the same as in "Eq. (3.33)" except that μ_p is replaced by $\mu_p(F)$, as the field and both currents drift in the same direction. Nevertheless, the diffusion current provided by "Eq. (3.35)" travels in both parallel and anti-parallel directions to the direction of the electric field. Also, the mobility resulting from the Einstein relation is included.

It can be observed from the continuity equation "Eq. (3.23)" that Δp^i can also be changed by additional contributions from trapping, recombination and generation. Thus putting all the terms together, the total change of Δp^i at position i is:

$$\begin{aligned}\Delta p^i = & -\Delta p_{drift}^{i\to i+1} - \Delta p_{drift}^{i\to i-1} + \Delta p_{driff}^{i\to i+1} - \Delta p_{driff}^{i\to i-1} + \Delta p_{drift}^{i-1\to i} + \Delta p_{drift}^{i+1\to i} + \Delta p_{driff}^{i-1\to i} \\ & + \Delta p_{driff}^{i+1\to i} - \Delta p_{rec}^{i} + \Delta p_{gen}^{i} - \Delta p_{trap}^{i} + \Delta p_{detrap}^{i}\end{aligned} \tag{3.37}$$

The total electrical current density J generated by all the charge carriers (particles) at position i can be calculated by:

$$J^i = J_n^i + J_p^i = \mathrm{e}\left(\frac{\partial p^{i\to i+1}}{\partial t^i} - \frac{\partial p^{i+1\to i}}{\partial t^i} - \frac{\partial n^{i\to i+1}}{\partial t^i} + \frac{\partial n^{i+1\to i}}{\partial t^i}\right)\Delta m \tag{3.38}$$

The discretized form of the continuity equation pertaining to the excitons "Eq. (3.27)" is written similarly to that of charge carriers.

Diffusion currents are described by an expression similar to "Eq. (3.35)" written as:

$$\frac{\partial s_{diff}^{i\to i+1}}{\partial t} = \frac{v_s}{\Delta m} s^i = \frac{D_s}{\Delta m^2} s^i = \frac{L_D^2}{\tau \Delta m^2} s^i \tag{3.39}$$

Excitons can undergo relaxation at a rate, of $1/\tau$, and get drained as a consequence. Exciton's density will change as a result of interactions such as: quenching or annihilation due to impurities and/or the addition of free charge carriers in the event where interaction rates and reaction cross-sections are available. The overall change of exciton's densities is written as:

$$\Delta s^i = \Delta s_{diff}^{i\to i+1} - \Delta s_{diff}^{i\to i-1} + \Delta s_{diff}^{i-1\to i} + \Delta s_{diff}^{i+1\to i} - \frac{1}{\tau} S_i + \Delta S_{gen_{opt}}^{i} - \Delta s_{quench}^{i} \tag{3.40}$$

Where $\Delta s_{gen_{opt}}^{i}$ is the optical generation term.

3.8 Time step calculation

To compute the updated values of the state variables, a time step Δt is required. It is necessary to optimize the time step since a too-large time step may cause instabilities while an excessively tiny time step will increase the number of iterations and thus raise the cost and duration of computations. Therefore, the inverse of the highest relative rate of change is used to determine an ideal Δt value in each iterative loop segment. This is expressed as:

$$\Delta t = \frac{min}{i}\left(\frac{1}{\sum \frac{\frac{\partial p^i_{drift,diff}}{\partial t}}{p^i}}, \frac{1}{\frac{\frac{\partial p^i_{rec}}{\partial t}}{p^i}}, \frac{1}{\frac{\frac{\partial p^i_{gen}}{\partial t}}{p^i}}, \frac{1}{\frac{\frac{\partial p^i_{(de)trap}}{\partial t}}{p^i}}, \dots \right) \tag{3.41}$$

In this case, the minimum overall current position i is chosen. "Eq. (3.40)" only displays the rates of change for the density of holes (p). For all rates of change pertaining to all state variables, such as electrons, holes, and excitons, the minimum is utilized. After determining the ideal value of Δt, the state variables' updated or new values are computed using;

$$p^{i,t_{j+1}} = p^{i,t_j} + \frac{\partial p^{i,t_j}}{\partial t}\Delta t^{t_j} \tag{3.42}$$

It can be observed that the equations for the densities n and s are similar. The initial values for the subsequent iteration step, which begins with the electric field computation once more, are the new or updated densities: n, p, and $s^{i,t_{j+1}}$.

4. RESULTS AND DISCUSSION

4.1 Simulation parameters

Here, we examine a random OPV device that has a bulk heterojunction (BHJ) encased in two metal contacts made of a combination of two materials, the donor and the acceptor. At this stage, we report our observations as with the processes within this arbitrary device, regarding charge carrier mobility and the recombination possibilities starting from the generation of an exciton to the collection of charges at the respective electrodes.

Table 1. Input parameters for the simulations. These values will fit experimental data of ZnPc:C60 bulk heterojunction solar cells

Parameter	Name	Value
E_{he}	Donor-acceptor transport gap	1.2eV
$N_C = N_V$	Effective density of states	$10^{21} cm^{-3}$
ε_r	Dielectric constant	5
d	Device thickness	50 nm
G	Optical generation rate	$1.5\times 10^{22} cm^{-3} s^{-1}$
$\emptyset_n = \emptyset_p$	Injection barriers	0.1/ 0.3 eV
T	temperature	300 K

The results presented below are obtained from a simulation of the drift-diffusion equations expressed in equations 3.22 to equation 3.28 . Both C++ and MATLAB and codes are written based on the algorithm presented above from equations 3.29 to equation 3.42. Table 1 shows the input parameters used in the simulation at a standard temperature conditions where T=300K.

4.2 Charge Carrier Mobility and the Open-Circuit Voltage

An organic bulk heterojunction (BHJ) photovoltaic device's efficiency is significantly influenced by the charge carrier mobility, or μ. This mobility is obtained based on the hopping rates between donor and acceptor molecules, which are influenced by the morphology of the intermixed layers as shown in "Fig.1". "Fig 1 (a)" shows the variation of Voc as a function of the mobility $\boldsymbol{\mu n} = \boldsymbol{\mu p}$; while "Fig 1 (b)" presents the trend of the FF as a function of the mobility $\boldsymbol{\mu n} = \boldsymbol{\mu p}$.

The charge carrier mobility μ has also been observed to influence the diffusion and recombination rates. One useful macroscopic parameter is the mobility that connects the electrical field and the effective drift velocity v in organic materials when hopping dominates transport. Consequently, a linear relationship between v and F can be expected. Another model will also incorporate a field, temperature, and charge carrier density dependency. A higher mobility (μ), which has been observed to increase charge-carrier extraction, will improve the efficiency (η) and, consequently, the fill factor (FF). The following recombination possibilities have been observed to exist in a bulk heterojunction (BHJ): μ can modify the recombination properties and cause losses, and μ has the ability to change either surface recombination of a charge carrier at the "wrong" electrode (hole at cathode, electron at anode) or bulk recombination, which occurs at a donor-acceptor interface inside the material. When Langevin recombination occurs, the open-circuit voltage (Voc) falls with μ.

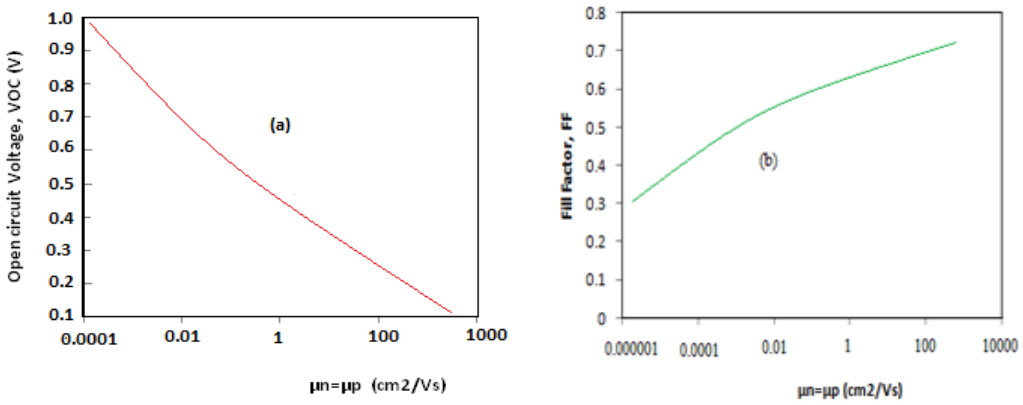

Fig 1: FF and Voc as a function of the mobility $\boldsymbol{\mu n} = \boldsymbol{\mu p}$

4.3 The effect of $\boldsymbol{np}$ on V_{oc} for charge carriers recombination

Based on "Fig. 2", it appears that the variation of V_{oc} with the product of electron and hole density (np) is logarithmic, as earlier found by (Centurioni, 2005). V_{oc} decreases as μ increases, lowering the device's charge carrier density and increasing extraction efficiency. The present investigation confirms that a higher μ leads to a lower np as long as there is a (drift) current flowing. However, this relationship does not hold at V_{oc} since there is no current flowing at that point, and no resulting charge extraction is taking place.

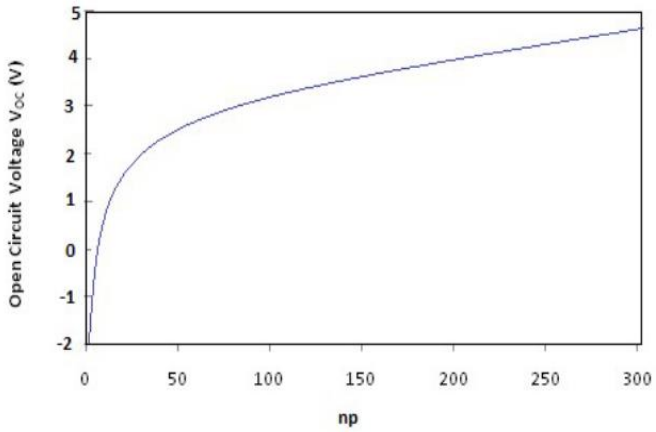

Fig 2. The behaviour of open circuit voltage with charge density.

4.4 Diffusion losses via layer thickness, d

Additional evidence on the diffusion losses may be seen in "Fig. 3," which shows the change of V_{oc} with layer thickness. The field inside the device decreases almost linearly with increasing thickness, which accounts for the V_{oc} against d connection. Consequently, the diffusion and drift currents that are balanced at V_{oc} will drop linearly with d. Since the diffusion gradient and the diffusion current are directly related, the latter will likewise drop linearly with d. A diminished diffusion gradient tallies with a diminished gradient in the quasi-Fermi levels, which have a logarithmic relationship with the charge carrier densities. As a result, the variation of this decreasing diffusion voltage, which is opposed to V_{oc}, with d will be logarithmic, explaining the observed rise in V_{oc}.

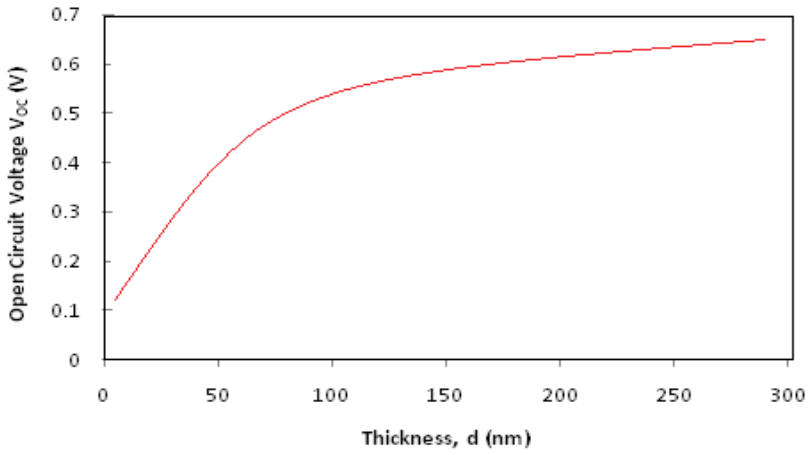

Fig 3. Open-circuit voltage with respect to layer thickness in a BHJ

This observed variation can be used as a basis to approximate the losses caused by recombination at the surface. It is advantageous to regulate the intensity of light to achieve a consistent average generation rate G, which can be determined by comparing the photo-current and the thickness, d. The correlation between V_{oc} and μ can be explained similarly where the losses caused by diffusion as earlier indicated are directly proportional to the mobility (μ).

4.4 Current-voltage (J-V) response with respect to charge mobility

In “Fig. (4)”, it is evident that Voc represents the voltage when there is no current flowing. As the mobility increases, due to the greater frequency of dark carrier recombination relative to carrier mobility,

V_{oc} decreases. This accounts for the discrepancy in behaviour observed between the short-circuit conditions at a voltage of approximately 0.6V and 0V. During the short-circuit condition, the bulk experiences less recombination as compared to the electrodes and the interface of the semiconductor where recombination is prevailing. The high intrinsic voltage during short-circuit situations prevents the diffusion of dark carriers in the bulk. Additionally, bulk recombination of photo-carriers decreases as carrier mobility rises. Nonetheless, low-mobility photo-carriers are poorly transported and collected by the electrodes. They rather build up within the bulk and may undergo recombination with other available photo-carriers. However, the losses attributed to the recombination current generated during the short-circuit condition are minimal. Meanwhile, recombination is prevalent both in the bulk and near the electrode at the 0.6V condition. In this circumstance, it is also observed that as mobility increases, the recombination of photo-carriers decreases while the recombination of dark carriers may increase.

The series resistance is one factor that affects the J-V curve as voltage increases in the forward bias. An increase in series resistance causes a drop in voltage. We can observe the effect of series resistance on the curve at the knee region when the voltage begins to increase as seen from voltages above 0.6V which get pronounced as voltage gets higher. Comparing the effect of series resistance on the PHJ, typical BHJ, OHJ and our BHJ simulation, we see that the effect of series resistance reduces based on our simulation seeing that it has the least gradient as voltage gets higher, indicating that the possibility of recombination reduces also. The effect of series resistance on the typical BHJ and PHJ are pronounced but more on a typical BHJ as seen in its high gradient leading to a fall in voltage at higher currents.

The shunt resistance affects the curve at lower (or negative voltage, -reverse bias). Shunt resistance causes an increase in leakage current in the region of reverse bias. This can be seen on the graph in which the J-V curve does not start at zero current density. The larger the shunt resistance, the smaller the current leakage. From the graph we can observe that the shunt resistance is greater in PHJ than in OHJ and a kind of averages in both the typical BHJ and in our simulation. The situation of shunt resistance from our study also proves that the possibility of recombination reduces since a high shunt resistance will reduce leakage current and reduce the possibility of recombination in the shunted path.

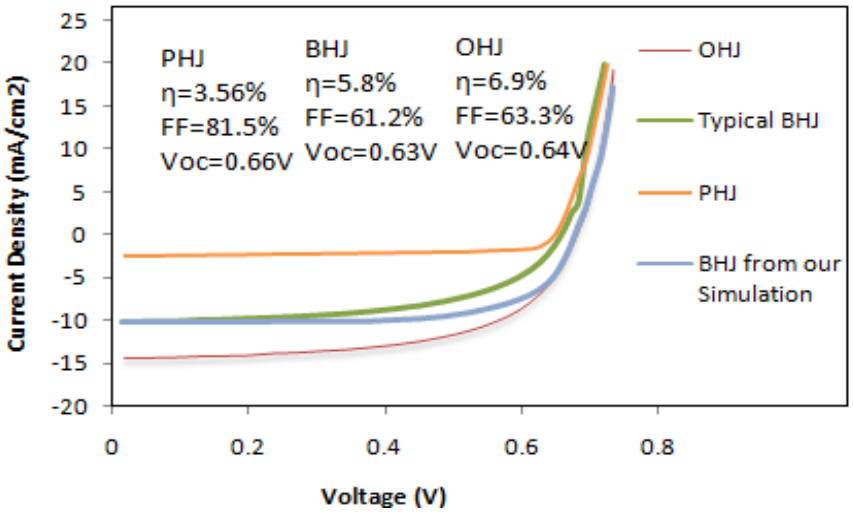

Fig 4. Current-voltage curve by simulation for a BHJ in Comparison to typical J–V characteristics for various OPV geometries: for planar heterojunction (PHJ), Bulk heterojunction (BHJ), ordered heterojunction (OHJ) OPV cell. (The typical J-V characteristics for OPV, BHJ and OHJ are from (Würfel et al., 2015).

The thickness of the device, as shown in "Fig. 4", also has an impact on the current density. There is an inverse proportionality relationship between the two. Additionally, the length of the active area and the

layer thickness, as depicted in "Fig. 5", are crucial factors in determining the efficiency of an organic solar device. While the thickness of the layer contributes to improving the efficiency, it can be effectively controlled in BHJ structures by increasing the thickness of the heterojunction while monitoring other parameters like the mobility and diffusivity of the organic solar cell. It is important to note that charge extraction at the electrode is not influenced by mobility. A shorter inter-electrodes distance will enhance faster extractions while minimizing the chances of recombination. Furthermore, we observed that there is an optimal average mobility that results in higher efficiency, suggesting a reduced likelihood of recombinations.

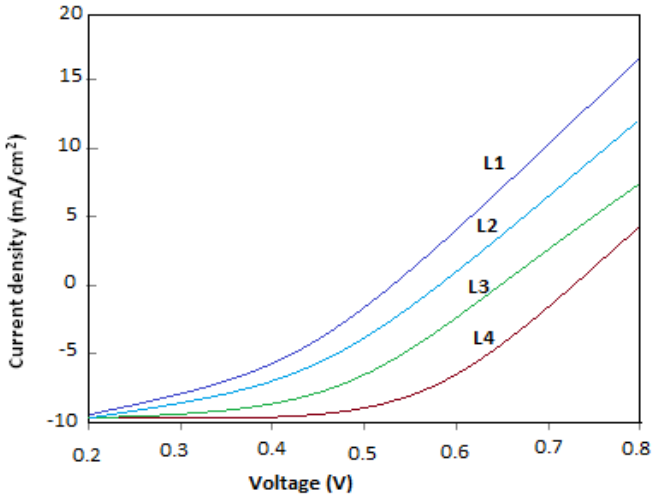

Fig 5. The behaviour of current density and voltage with increasing thickness of the device. The thickness $\boldsymbol{L_4} > \boldsymbol{L_3} > \boldsymbol{L_2} > \boldsymbol{L_1}$

4.5 The effect of density of state and energy on charge recombination

The mobile charge carriers in organic semiconductors are represented by a Gaussian density of states (DOS) expressed as;

$$N_{guass}(E) = \frac{N_0}{\sqrt{2\pi\delta^2}} exp\left[-\left(\frac{E-E_0}{\sqrt{2}\delta}\right)^2\right] \tag{4.1}$$

Where: E_0 is the reference energy level, which characterizes both the trapped and the free carriers, N_0 is the site density, and δ is the Gaussian width.

In general, the active layers in OPVs are usually characterized by an energetic disorder given their solution-based preparations. As a result, the HOMO and LUMO of the active layer exhibit a distinct energetic distribution, which can be represented by a Gaussian density of states "Eq. (4.1)" and illustrated in "Fig. 6".

When the device is exposed to sufficiently energetic light, it overcomes easily the energy gap and exciton binding energy, resulting in an increase in mobility and hence, efficiency. Therefore, a high sun is necessary for the BHJ to perform optimally. However, if the energy of the incident light spectrum is less than 1.2eV, an insufficient number of excitons will be generated with the appropriate energy to escape the dark carriers. In such cases, the few charge carriers present may either undergo germinate recombination or they may undergo recombination with the dark carriers at the electrode if they happen to cross the heterojunction. Conversely, if the light is highly energetic above 4.5eV, it will assist in high mobility, which may lead to quick recombination.

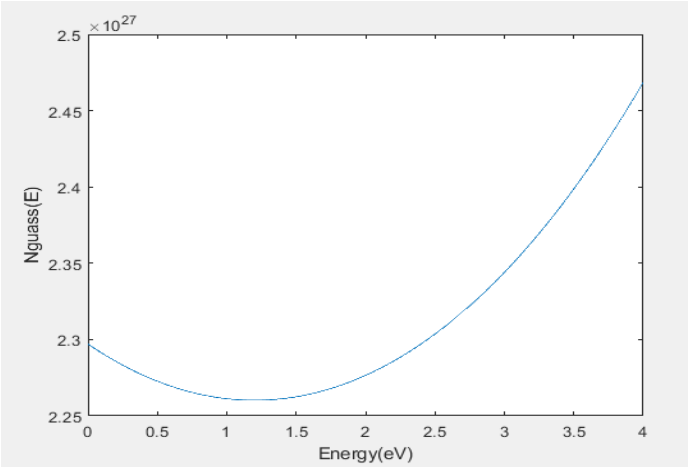

Fig 6. Gaussian density of State with respect to energy

In the case of perovskite solar cells, recombination processes can be reduced by using materials exhibiting high quality hole and electron transport (Liu & Johnston, 2013) and by improving the energy level alignment within the transport layers of the perovskites, (Zhao & Zhang, 2020) This will facilitate charge carrier mobility and reduce the distance charge carriers should travel, (Sahiba & Matsui, 2016) such that charge carriers get to the electrodes fast enough before recombination takes place. The contact interface between the electrode layers and the perovskite layers can be made of high quality by using buffer layers (Chen & Zhao, 2020) to enhance quick extractions at the electrodes before the occurrence of recombination.

5. CONCLUSION

It is clear from this work that the carrier density affects the charge carrier recombination rate in a BHJ solar cell. The applied voltage determines the device's carrier density. The internal field created by the built-in voltage diminishes as the forward bias voltage progressively rises, increasing the carrier density. The voltage at which the recombination rate exactly equals the photogeneration rate is denoted by V_{oc}. Our simulation tests have shown that a BHJ solar cell can have a little greater mobility value than usual, which, if maintained, can greatly increase its efficiency. Recombination in the device limits V_{oc}, which is highly reliant on μ in recombination processes. Additionally, μ affects the recombination constants. V_{oc} will be controlled by the dynamics of the CT state rather than the recombination coefficients of free charge carriers if the creation and recombination of free charge carriers take place through this state. This allows for the control of the system's effective mobility. Thus, we can significantly lower recombination in a bulk heterojunction solar cell by preserving charge carrier mobility within the ideal range, which is also dependent on the Gaussian density of state and the characteristics of the donor and acceptor in the device.

NOMENCLATURE

D	Diffusivity constant [cm/s]	T	Temperature [K]
e	Electronic charge[C]	v	Drift velocity [cm/s]
E	Electric force [N]	V	Applied bias voltage [V]
f	Distribution function	V_{bi}	Built-in voltage [V]
E_F^n	Electrochemical potential gradient [V]	v_n	Electron average velocity [m/s]

F	Electric field strength [N/C]	v_p	Holes average velocity [m/s]
G	Charge carrier generation	s	Gradient in the diffusion current changes
G_{opt}	Optical generation term [$cm^{-3}s$]	β_L	Langevin recombination coefficient
j	Electric current density [mA/cm^2]	σ	Conductivity [(S/m)]
J_n	Electron current density [mA/cm^2]	μ_+	Hole mobility [$m^2/(V{\cdot}s)$]
J_p	Hole current density [mA/cm^2]	ε_0	Permittivity of free space [F/m]
j^n_{diff}	Electron diffusion current [cm^2/s]	ε	Relative permittivity [F/m]
j^p_{diff}	Hole diffusion current [cm^2/s]	ε_r	Dielectric constant
k_B	Boltzmann constant [eV/K]	$\emptyset$	Electrical potential [eV]
L_D	Exciton diffusion length [nm]	η	Electrochemical potential [eV/C]
n	Electron density [mA/cm^2]	μ_-	Electron mobility [cm^2/Vs]
p	Holes density [mA/cm^2]	μ	Synchronised mobility [cm^2/Vs]
N_D^+	Positive ionized dopant density [cm^{-3}]	τ_r	Average scattering time [ns]
N_A^-	Negative ionized dopant density [cm^{-3}]	τ	Exciton lifetime[ns]
OPV	Organic photovoltaic	τ_s	Scattering time [ns]
PV	Photovoltaic	ξ_n	Electron concentration gradient
R	Charge carrier recombination	ξ_p	Hole concentration gradient

REFERENCES

Abudulimu, A. (2012). *Measuring the efficiency and charge carrier mobility of organic solar cells* [Umeå University]. http://oatd.org/oatd/record?record=oai%5C%3ADiVA.org%5C%3Aumu-63805

Bi, Z., Zhu, Q., Xu, X., Naveed, H. B., Sui, X., Xin, J., Zhang, L., Li, T., Zhou, K., Liu, X., Zhan, X., & Ma, W. (2019). Efficient Quaternary Organic Solar Cells with Parallel Alloy Morphology. *Advanced Functional Materials*, *29*(9), 1806804. https://doi.org/10.1002/adfm.201806804

Centurioni, E. (2005). Generalized matrix method for calculation of internal light energy flux in mixed coherent and incoherent multilayers. *Applied Optics*, *44*(35), 7532. https://doi.org/10.1364/AO.44.007532

Chen, L. X. (2019). Organic Solar Cells: Recent Progress and Challenges. *ACS Energy Letters*, *4*(10), 2537–2539. https://doi.org/10.1021/acsenergylett.9b02071

Chen, W., Yin, W., & Zhao, L. (2020) Buffer layers for perovskite solar cells: from materials to interface engineering . Journal of Materials chemistry A, 8(7), 3536-3551. DOI: 10. 1039/C9TA12733H

Cui, Y., Yao, H., Zhang, J., Xian, K., Zhang, T., Hong, L., Wang, Y., Xu, Y., Ma, K., An, C., He, C., Wei, Z., Gao, F., & Hou, J. (2020). Single-Junction Organic Photovoltaic Cells with Approaching 18% Efficiency. *Advanced Materials (Deerfield Beach, Fla.)*, *32*(19), e1908205. https://doi.org/10.1002/adma.201908205

Dastoor, P. C., & Belcher, W. J. (2019). How the West was Won? A History of Organic Photovoltaics. *Substantia*, 99-110 Pages. https://doi.org/10.13128/SUBSTANTIA-612

Duan, L., & Uddin, A. (2020). Progress in Stability of Organic Solar Cells. *Advanced Science*, *7*(11), 1903259. https://doi.org/10.1002/advs.201903259

Fan, B., Ying, L., Wang, Z., He, B., Jiang, X.-F., Huang, F., & Cao, Y. (2017). Optimisation of processing solvent and molecular weight for the production of green-solvent-processed all-polymer

solar cells with a power conversion efficiency over 9%. *Energy & Environmental Science*, *10*(5), 1243–1251. https://doi.org/10.1039/C7EE00619E

Forrest, S. (2012). Energy efficiency with organic electronics: Ching W. Tang revisits his days at Kodak. *MRS Bulletin*, *37*(6), 552–553. https://doi.org/10.1557/mrs.2012.125

Galagan, Y., & Andriesse, R. (2012). Organic Photovoltaics: Technologies and Manufacturing. In V. Fthenakis (Ed.), *Third Generation Photovoltaics*. InTech. https://doi.org/10.5772/25901

Gao, L., Zhang, Z.-G., Xue, L., Min, J., Zhang, J., Wei, Z., & Li, Y. (2016). All-Polymer Solar Cells Based on Absorption-Complementary Polymer Donor and Acceptor with High Power Conversion Efficiency of 8.27%. *Advanced Materials (Deerfield Beach, Fla.)*, *28*(9), 1884–1890. https://doi.org/10.1002/adma.201504629

Goh, T., Huang, J. S., Yager, K. G., Sfeir, M. Y., Nam, C. Y., Tong, X., Guard, L. M., Melvin, P. R., Antonio, F., Bartolome, B. G., Lee, M. L., Hazari, N., & Taylor, A. D. (2016). Quaternary Organic Solar Cells Enhanced by Cocrystalline Squaraines with Power Conversion Efficiencies >10%. *Advanced Energy Materials*, *6*(21). https://doi.org/10.1002/aenm.201600660

Göhler, C., Wagenpfahl, A., & Deibel, C. (2018). Nongeminate Recombination in Organic Solar Cells. *Advanced Electronic Materials*, *4*(10), 1700505. https://doi.org/10.1002/aelm.201700505

Groves, C., Blakesley, J. C., & Greenham, N. C. (2010). Effect of Charge Trapping on Geminate Recombination and Polymer Solar Cell Performance. *Nano Letters*, *10*(3), 1063–1069. https://doi.org/10.1021/nl100080r

Guo, Y., Li, Y., Awartani, O., Han, H., Zhao, J., Ade, H., Yan, H., & Zhao, D. (2017). Improved Performance of All-Polymer Solar Cells Enabled by Naphthodiperylenetetraimide-Based Polymer Acceptor. *Advanced Materials (Deerfield Beach, Fla.)*, *29*(26). https://doi.org/10.1002/adma.201700309

Guo, Y., Li, Y., Awartani, O., Zhao, J., Han, H., Ade, H., Zhao, D., & Yan, H. (2016). A Vinylene Bridged Perylenediimide Based Polymeric Acceptor Enabling Efficient All Polymer Solar Cells Processed under Ambient Conditions. *Advanced Materials*, *28*(38), 8483–8489. https://doi.org/10.1002/adma.201602387

Hong, L., Yao, H., Cui, Y., Ge, Z., & Hou, J. (2020). Recent advances in high-efficiency organic solar cells fabricated by eco-compatible solvents at relatively large-area scale. *APL Materials*, *8*(12), 120901. https://doi.org/10.1063/5.0027948

Jin, K., Xiao, Z., & Ding, L. (2021). D18, an eximious solar polymer! *Journal of Semiconductors*, *42*(1), 010502. https://doi.org/10.1088/1674-4926/42/1/010502

Li, C., Zhou, J., Song, J., Xu, J., Zhang, H., Zhang, X., Guo, J., Zhu, L., Wei, D., Han, G., Min, J., Zhang, Y., Xie, Z., Yi, Y., Yan, H., Gao, F., Liu, F., & Sun, Y. (2021). Non-fullerene acceptors with branched side chains and improved molecular packing to exceed 18% efficiency in organic solar cells. *Nature Energy*, *6*(6), 605–613. https://doi.org/10.1038/s41560-021-00820-x

Li, S., Ye, L., Zhao, W., Zhang, S., Mukherjee, S., Ade, H., & Hou, J. (2016). Energy Level Modulation of Small Molecule Electron Acceptors to Achieve over 12% Efficiency in Polymer Solar Cells. *Advanced Materials*, *28*(42), 9423–9429. https://doi.org/10.1002/adma.201602776

Li, Y., Huang, W., Zhao, D., Wang, L., Jiao, Z., Huang, Q., Wang, P., Sun, M., & Yuan, G. (2022). Recent Progress in Organic Solar Cells: A Review on Materials from Acceptor to Donor. *Molecules*, *27*(6), 1800. https://doi.org/10.3390/molecules27061800

Lin, Y., Wang, J., Zhang, Z., Bai, H., Li, Y., Zhu, D., & Zhan, X. (2015). An Electron Acceptor Challenging Fullerenes for Efficient Polymer Solar Cells. *Advanced Materials*, *27*(7), 1170–1174. https://doi.org/10.1002/adma.201404317

Lin, Y., Zhao, F., He, Q., Huo, L., Wu, Y., Parker, T. C., Ma, W., Sun, Y., Wang, C., Zhu, D., Heeger, A. J., Marder, S. R., & Zhan, X. (2016). High-Performance Electron Acceptor with Thienyl Side Chains for Organic Photovoltaics. *Journal of the American Chemical Society*, *138*(14), 4955–4961. https://doi.org/10.1021/jacs.6b02004

Liu, M., Johnston, M., & Snaith, H. (2013). Efficient planar heterojunction perovskite solar cells by vapor deposition. Nature, 501(7467), 395-398.DOI:[10. 1038./nature12509] (https://doi. org/10.1038)

Liu, Q., Jiang, Y., Jin, K., Qin, J., Xu, J., Li, W., Xiong, J., Liu, J., Xiao, Z., Sun, K., Yang, S., Zhang, X., & Ding, L. (2020). 18% Efficiency organic solar cells. *Science Bulletin*, *65*(4), 272–275. https://doi.org/10.1016/j.scib.2020.01.001

Ma, R., Liu, T., Luo, Z., Guo, Q., Xiao, Y., Chen, Y., Li, X., Luo, S., Lu, X., Zhang, M., Li, Y., & Yan, H. (2020). Improving open-circuit voltage by a chlorinated polymer donor endows binary organic solar cells efficiencies over 17%. *Science China Chemistry*, *63*(3), 325–330. https://doi.org/10.1007/s11426-019-9669-3

Mahmud, M., Huda, N., Farjana, S., & Lang, C. (2018). Environmental Impacts of Solar-Photovoltaic and Solar-Thermal Systems with Life-Cycle Assessment. *Energies*, *11*(9), 2346. https://doi.org/10.3390/en11092346

Mandal, S., Purohit, G., & Katiyar, M. (2012). Inkjet Printed Organic Thin Film Transistors: Achievements and Challenges. *Materials Science Forum*, *736*, 250–274. https://doi.org/10.4028/www.scientific.net/MSF.736.250

Markus, B., & Anne, K. (2009). *Positivity Preserving Discretization of Time Dependent Semiconductor Model Equations* (6). Norwegian University of Science and Technology, N-7491. https://www.math.ntnu.no/preprint/numerics/2009/N6-2009.pdf

Mori, D., Benten, H., Okada, I., Ohkita, H., & Ito, S. (2014). Low Bandgap Donor/Acceptor Polymer Blend Solar Cells with Efficiency Exceeding 4%. *Advanced Energy Materials*, *4*(3), 1301006. https://doi.org/10.1002/aenm.201301006

Qin, J., Zhang, L., Zuo, C., Xiao, Z., Yuan, Y., Yang, S., Hao, F., Cheng, M., Sun, K., Bao, Q., Bin, Z., Jin, Z., & Ding, L. (2021). A chlorinated copolymer donor demonstrates a 18.13% power conversion efficiency. *Journal of Semiconductors*, *42*(1), 010501. https://doi.org/10.1088/1674-4926/42/1/010501

Saliba, M Matsui, T., Domanski,K., et al. (2016). Interfacial engineering for high efficiency perovskite solar cells. Science, 354(6308), 206-209. DOI:[10.1126/science.aaf3503] (https://doi.org /10. 1126)

Schopp, N., Akhtanova, G., Panoy, P., Arbuz, A., Chae, S., Yi, A., Kim, H. J., Promarak, V., Nguyen, T.-Q., & Brus, V. V. (2022). Unraveling Device Physics of Dilute-Donor Narrow-Bandgap Organic Solar Cells with Highly Transparent Active Layers. *Advanced Materials (Deerfield Beach, Fla.)*, *34*(31), e2203796. https://doi.org/10.1002/adma.202203796

Shaabani, L., Blom, P., & Havenith, R. (2012). *Advanced device structures for enhanced organic solar cell efficiencies*. https://www.semanticscholar.org/paper/Advanced-device-structures-for-enhanced-organic-Shaabani-Blom/91e7a532fd5cd7004a9b648bf3ad413c41061533#citing-papers

Sharma, A., Masoumi, S., Gedefaw, D., O'Shaughnessy, S., Baran, D., & Pakdel, A. (2022). Flexible solar and thermal energy conversion devices: Organic photovoltaics (OPVs), organic thermoelectric generators (OTEGs) and hybrid PV-TEG systems. *Applied Materials Today*, *29*, 101614. https://doi.org/10.1016/j.apmt.2022.101614

Shi, Y., Guo, H., Huang, J., Zhang, X., Wu, Z., Yang, K., Zhang, Y., Feng, K., Woo, H. Y., Ortiz, R. P., Zhou, M., & Guo, X. (2020). Distannylated Bithiophene Imide: Enabling High-Performance n-Type Polymer Semiconductors with an Acceptor-Acceptor Backbone. *Angewandte Chemie (International Ed. in English)*, *59*(34), 14449–14457. https://doi.org/10.1002/anie.202002292

Song, J., Zhu, L., Li, C., Xu, J., Wu, H., Zhang, X., Zhang, Y., Tang, Z., Liu, F., & Sun, Y. (2021). High-efficiency organic solar cells with low voltage loss induced by solvent additive strategy. *Matter*, *4*(7), 2542–2552. https://doi.org/10.1016/j.matt.2021.06.010

Street, R. A., Krakaris, A., & Cowan, S. R. (2012). Recombination Through Different Types of Localized States in Organic Solar Cells. *Advanced Functional Materials*, *22*(21), 4608–4619. https://doi.org/10.1002/adfm.201200031

Sun, H., Yu, H., Shi, Y., Yu, J., Peng, Z., Zhang, X., Liu, B., Wang, J., Singh, R., Lee, J., Li, Y., Wei, Z., Liao, Q., Kan, Z., Ye, L., Yan, H., Gao, F., & Guo, X. (2020). A Narrow Bandgap n-Type Polymer with an Acceptor–Acceptor Backbone Enabling Efficient All Polymer Solar Cells. *Advanced Materials*, *32*(43), 2004183. https://doi.org/10.1002/adma.202004183

Tang, C.W. (1986). Two-layer organic photovoltaic cell Applied Physical Letters. 48 (2): 183–185. https://doi.org/10.1063/1.96937

Tran, H. N., Park, S., Wibowo, F. T. A., Krishna, N. V., Kang, J. H., Seo, J. H., Nguyen Phu, H., Jang, S., & Cho, S. (2020). 17% Non Fullerene Organic Solar Cells with Annealing Free Aqueous MoO_x. *Advanced Science*, *7*(21), 2002395. https://doi.org/10.1002/advs.202002395

Vollbrecht, J., Lee, J., Ko, S.-J., Brus, V. V., Karki, A., Le, W., Seifrid, M., Ford, M. J., Cho, K., Bazan, G. C., & Nguyen, T.-Q. (2020). Design of narrow bandgap non-fullerene acceptors for photovoltaic applications and investigation of non-geminate recombination dynamics. *Journal of Materials Chemistry C*, *8*(43), 15175–15182. https://doi.org/10.1039/D0TC02136A

Vollbrecht, J., Tokmoldin, N., Sun, B., Saglamkaya, E., Perdigón-Toro, L., Hosseini, S. M., Son, J. H., Woo, H. Y., Shoaee, S., & Neher, D. (2023). On the relationship of the effective mobility and photoconductance mobility in organic solar cells. *Energy Advances*, *2*(9), 1390–1398. https://doi.org/10.1039/D3YA00125C

Volpi, R. (2017, January 16). *Modelling Charge Transport for Organic Solar Cells within Marcus Theory*. https://doi.org/10.3384/diss.diva-133329

Wagenpfahl, A., Deibel, C., & Dyakonov, V. (2010). Organic solar cell efficiencies under the aspect of reduced surface recombination velocities. *IEEE Journal of Selected Topics in Quantum Electronics*, *16*(6), 1759–1763. https://doi.org/10.1109/JSTQE.2010.2042142

Wang, J.-L., Liu, K.-K., Hong, L., Ge, G.-Y., Zhang, C., & Hou, J. (2018). Selenopheno[3,2- *b*]thiophene-Based Narrow-Bandgap Nonfullerene Acceptor Enabling 13.3% Efficiency for Organic Solar Cells with Thickness-Insensitive Feature. *ACS Energy Letters*, *3*(12), 2967–2976. https://doi.org/10.1021/acsenergylett.8b01808

Wilken, S., Scheunemann, D., Dahlström, S., Nyman, M., Parisi, J., & Österbacka, R. (2021). How to Reduce Charge Recombination in Organic Solar Cells: There Are Still Lessons to Learn from P3HT:PCBM. *Advanced Electronic Materials*, *7*(5), 2001056. https://doi.org/10.1002/aelm.202001056

Würfel, U., Neher, D., Spies, A., & Albrecht, S. (2015). Impact of charge transport on current-voltage characteristics and power-conversion efficiency of organic solar cells. *Nature Communications*, *6*(1), 6951. https://doi.org/10.1038/ncomms7951

Xu, X., Bi, Z., Ma, W., Wang, Z., Choy, W. C. H., Wu, W., Zhang, G., Li, Y., & Peng, Q. (2017). Highly Efficient Ternary-Blend Polymer Solar Cells Enabled by a Nonfullerene Acceptor and Two Polymer

Donors with a Broad Composition Tolerance. *Advanced Materials (Deerfield Beach, Fla.)*, *29*(46). https://doi.org/10.1002/adma.201704271

Xu, X., Yu, T., Bi, Z., Ma, W., Li, Y., & Peng, Q. (2018). Realizing Over 13% Efficiency in Green Solvent Processed Nonfullerene Organic Solar Cells Enabled by 1,3,4 Thiadiazole Based Wide Bandgap Copolymers. *Advanced Materials*, *30*(3), 1703973. https://doi.org/10.1002/adma.201703973

Yuan, J., Huang, T., Cheng, P., Zou, Y., Zhang, H., Yang, J. L., Chang, S.-Y., Zhang, Z., Huang, W., Wang, R., Meng, D., Gao, F., & Yang, Y. (2019). Enabling low voltage losses and high photocurrent in fullerene-free organic photovoltaics. *Nature Communications*, *10*(1), 570. https://doi.org/10.1038/s41467-019-08386-9

Yuan, J., Zhang, Y., Zhou, L., Zhang, G., Yip, H.-L., Lau, T.-K., Lu, X., Zhu, C., Peng, H., Johnson, P. A., Leclerc, M., Cao, Y., Ulanski, J., Li, Y., & Zou, Y. (2019). Single-Junction Organic Solar Cell with over 15% Efficiency Using Fused-Ring Acceptor with Electron-Deficient Core. *Joule*, *3*(4), 1140–1151. https://doi.org/10.1016/j.joule.2019.01.004

Yumnam, N., Hirwa, H., & Wagner, V. (2017). Analytical and numerical analysis of charge carriers extracted by linearly increasing voltage in a metal-insulator-semiconductor structure relevant to bulk heterojunction organic solar cells. *Journal of Physics D: Applied Physics*, *50*(49), 495107. https://doi.org/10.1088/1361-6463/aa94f1

Zhan, X., Tan, Z., Domercq, B., An, Z., Zhang, X., Barlow, S., Li, Y., Zhu, D., Kippelen, B., & Marder, S. R. (2007). A High-Mobility Electron-Transport Polymer with Broad Absorption and Its Use in Field-Effect Transistors and All-Polymer Solar Cells. *Journal of the American Chemical Society*, *129*(23), 7246–7247. https://doi.org/10.1021/ja071760d

Zhang, S., Qin, Y., Zhu, J., & Hou, J. (2018). Over 14% Efficiency in Polymer Solar Cells Enabled by a Chlorinated Polymer Donor. *Advanced Materials (Deerfield Beach, Fla.)*, *30*(20), e1800868. https://doi.org/10.1002/adma.201800868

Zhao, R., Wang, N., Yu, Y., & Liu, J. (2020). Organoboron Polymer for 10% Efficiency All-Polymer Solar Cells. *Chemistry of Materials*, *32*(3), 1308–1314. https://doi.org/10.1021/acs.chemmater.9b04997

Zhao, W., Li, S., Yao, H., Zhang, S., Zhang, Y., Yang, B., & Hou, J. (2017). Molecular Optimization Enables over 13% Efficiency in Organic Solar Cells. *Journal of the American Chemical Society*, *139*(21), 7148–7151. https://doi.org/10.1021/jacs.7b02677

Zhao, W., Qian, D., Zhang, S., Li, S., Inganäs, O., Gao, F., & Hou, J. (2016). Fullerene Free Polymer Solar Cells with over 11% Efficiency and Excellent Thermal Stability. *Advanced Materials*, *28*(23), 4734–4739. https://doi.org/10.1002/adma.201600281

Zhao, Y., & Zhang, Z. (2020).Recent progress on charge transport layers in perovskite solar cells: strategies and challenges. Energy and environment science, 13(4), 1110-1138. DOI[10.1039 /C9EE03717H]

Zheng, Z., Awartani, O. M., Gautam, B., Liu, D., Qin, Y., Li, W., Bataller, A., Gundogdu, K., Ade, H., & Hou, J. (2017). Efficient Charge Transfer and Fine-Tuned Energy Level Alignment in a THF-Processed Fullerene-Free Organic Solar Cell with 11.3% Efficiency. *Advanced Materials (Deerfield Beach, Fla.)*, *29*(5). https://doi.org/10.1002/adma.201604241

Zojer, K. (2021). Simulation of Charge Carriers in Organic Electronic Devices: Methods with their Fundamentals and Applications. *Advanced Optical Materials*, *9*(14), 2100219. https://doi.org/10.1002/adom.202100219